

Crystal structure of aprocitentan Form A, C₁₆H₁₄Br₂N₆O₄S

James A. Kaduk^{1,2} , Anja Dosen³  and Tom N. Blanton³ 

¹Department of Chemistry, Illinois Institute of Technology, Chicago, IL, USA

²Department of Physics, North Central College, Naperville, IL, USA

³International Centre for Diffraction Data (ICDD), Newtown Square, PA, USA

(Received 21 December 2024; revised 25 February 2025; accepted 19 March 2025)

Abstract: The crystal structure of aprocitentan Form A has been solved and refined using synchrotron X-ray powder diffraction data and optimized using density functional theory techniques. Aprocitentan Form A crystallizes in space group *P*-1 (#2) with *a* = 11.7381(11), *b* = 10.6771(12), *c* = 9.6624(5) Å, α = 110.4365(13), β = 92.3143(13), γ = 113.513(2)°, *V* = 1,017.53(5) Å³, and *Z* = 2 at 298 K. The crystal structure consists of layers of aprocitentan molecules, approximately along the 1,-7,7 plane. N–H⋯N hydrogen bonds link the molecules within these layers. The powder pattern has been submitted to the International Centre for Diffraction Data for inclusion in the Powder Diffraction File™.

© The Author(s), 2025. Published by Cambridge University Press on behalf of International Centre for Diffraction Data. This is an Open Access article, distributed under the terms of the Creative Commons Attribution licence (<http://creativecommons.org/licenses/by/4.0>), which permits unrestricted re-use, distribution and reproduction, provided the original article is properly cited. [doi:10.1017/S088571562500017X]

Key words: aprocitentan, Tryvio™, crystal structure, Rietveld refinement, density functional theory

I. INTRODUCTION

Aprocitentan (sold under the brand name Tryvio™) is used to treat hypertension (high blood pressure). Aprocitentan functions as a receptor antagonist targeting endothelin A and B receptors. The systematic name (CAS Registry Number 1103522-45-7) is 5-(4-bromophenyl)-4-[2-(5-bromopyrimidin-2-yl)oxyethoxy]-6-(sulfamoylamino)pyrimidine. A two-dimensional molecular diagram of aprocitentan is shown in Figure 1.

Aprocitentan and processes for its preparation are claimed in U.S. Patent 8324232 B2 (Bolli et al., 2012; Actelion Pharmaceuticals Ltd.). Crystalline Forms A, C, D, E (acetonitrile solvate), J, K (DMSO solvate), and L (ethanol solvate) are claimed in International Patent Application WO 2018/154101 A1 (Bolli et al., 2018; Idorsia Pharmaceuticals Ltd.). The U.S. equivalent is US 2020/0002317 A1 (Bolli et al., 2020; Idorsia Pharmaceuticals Ltd.). A new crystalline form of aprocitentan is claimed in International Patent Application WO 2021/088645 A1 (Chen and Zhu, 2021; Crystal Pharmaceutical [Suzhou] Co.). Several other crystalline forms of aprocitentan and solvates are claimed in International Patent Application WO 2021/237004 A1 (Bibulić and Matečić, 2021; Teva Pharmaceuticals).

This work was carried out as part of a project (Kaduk et al., 2014) to determine the crystal structures of large-volume commercial pharmaceuticals and include high-quality powder diffraction data for them in the Powder Diffraction File (PDF®; Kabekkodu et al., 2024).

II. EXPERIMENTAL

Aprocitentan was a commercial reagent, purchased from TargetMol (Batch #T7817) and was used as received. The white powder was packed into a 0.5-mm-diameter Kapton capillary and rotated during the measurement at ~2 Hz. The powder pattern was measured at 298(1) K at the Wiggler Low Energy Beamline (Leontowich et al., 2021) of the Brockhouse X-Ray Diffraction and Scattering Sector of the Canadian Light Source using a wavelength of 0.819826(2) Å (15.1 keV) from 1.6 to 75.0° 2θ with a step size of 0.0025° and a collection time of 3 minutes. The high-resolution powder diffraction data were collected using eight Dectris Mythen2 X series 1K linear strip detectors. NIST SRM 660b LaB₆ was used to calibrate the instrument and refine the monochromatic wavelength used in the experiment.

The pattern was indexed using N-TREOR as incorporated into EXPO2014 (Altomare et al., 2013) on a primitive triclinic unit cell with *a* = 11.74097, *b* = 10.68446, *c* = 9.66628 Å, α = 110.461, β = 92.278, γ = 113.498°, *V* = 1,019.0 Å³, and *Z* = 2. The space group was assumed to be *P*-1, which was confirmed by the successful solution and refinement of the structure. A reduced cell search of the Cambridge Structural Database (Groom et al., 2016) yielded one hit, but no structures of aprocitentan or its derivatives.

An aprocitentan molecule was downloaded from PubChem (Kim et al., 2023) as Conformer3D_COMPOUND_CID_25099191.sdf. It was converted to a *.mol2 file using Mercury (Macrae et al., 2020). The crystal structure was solved using Monte Carlo simulated annealing techniques as implemented in EXPO2014 (Altomare et al., 2013). For the structure solution, a pattern with 100,000 counts subtracted from each point was used.

Corresponding author: James A. Kaduk; Email: kaduk@polycrystallography.com

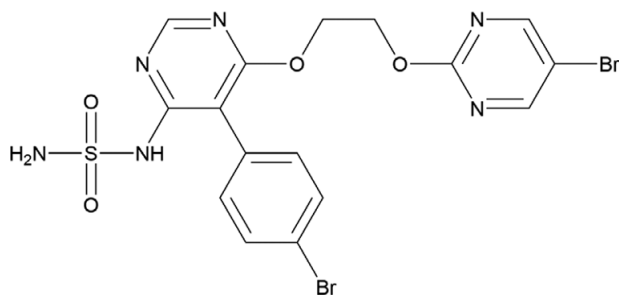


Figure 1. The two-dimensional structure of aprocitentan.

Rietveld refinement was carried out with GSAS-II (Toby and Von Dreele, 2013). Only the 4.0 to 40.0° portion of the pattern was included in the refinements ($d_{\min} = 1.198 \text{ \AA}$). The specimen is highly absorbing in addition to fluorescing, so an absorption model of $\mu R = 0.87$ (calculated using the tool on the 11-BM website) was included. All non-H-bond distances and angles were subjected to restraints, based on a Mercury/Mogul Geometry Check (Bruno et al., 2004; Sykes et al., 2011). The Mogul average and standard deviation for each quantity were used as the restraint parameters. The three aromatic rings were restrained to be planar. The restraints contributed 3.6% to the overall χ^2 . Most of the hydrogen atoms were included in calculated positions, which were recalculated during the refinement using Materials Studio (Dassault Systèmes, 2023). The positions of the H atoms H40 and H41 of the sulfonamide group were refined, subject to bond distance and angle restraints. The two Br atoms were refined anisotropically. The U_{iso} of the other heavy atoms were grouped by chemical similarity. The U_{iso} for the H atoms were fixed at $1.3 \times$ the U_{iso} of the heavy atoms to which they are attached. The peak profiles were described using an isotropic microstrain model. The background was modeled using a six-term shifted Chebyshev polynomial, with a peak at

10.92° to model the scattering from the Kapton capillary and any amorphous component.

The final refinement of 132 variables using 14,401 observations and 77 restraints yielded the residual $R_{\text{wp}} = 0.00934$. The exceptionally low R_{wp} results from the high background (from Br fluorescence), which is fitted very well. The largest peak (0.84 Å from N9) and hole (0.59 Å from O7) in the difference Fourier map were 0.45(11) and $-0.44(11) e\text{\AA}^{-3}$, respectively. The final Rietveld plot is shown in Figure 2. The largest features in the normalized error plot are in the positions and shapes of some of the strong low-angle peaks. These misfits probably indicate subtle changes in the specimen during the measurement. It would be surprising if a molecule that contains two C–Br bonds did not exhibit beam damage.

The crystal structure of aprocitentan was optimized (fixed experimental unit cell) with density functional theory techniques using VASP 6.0 (Kresse and Furthmüller, 1996) through the MedeA graphical interface (Materials Design, 2024). The calculation was carried out on 32 cores of a 144-core (768-GB memory) HPE Superdome Flex 280 Linux server at North Central College. The calculation used the GGA-PBE functional, a plane wave cutoff energy of 400.0 eV, and a k -point spacing of 0.5 \AA^{-1} , leading to a $2 \times 2 \times 2$ mesh, and took ~4.7 hours. Single-point density functional calculations (fixed experimental cell) and population analysis were carried out using CRYSTAL23 (Erba et al., 2023). The basis sets for the H, C, and O atoms in the calculation were those of Gatti et al. (1994), and the basis sets for S and Br were those of Peintinger et al. (2013). The calculations were run on a 3.5-GHz PC using eight k -points and the B3LYP functional and took ~2.3 hours.

III. RESULTS AND DISCUSSION

This synchrotron powder pattern of aprocitentan matches the diffraction pattern reported for Form A by Bolli et al.

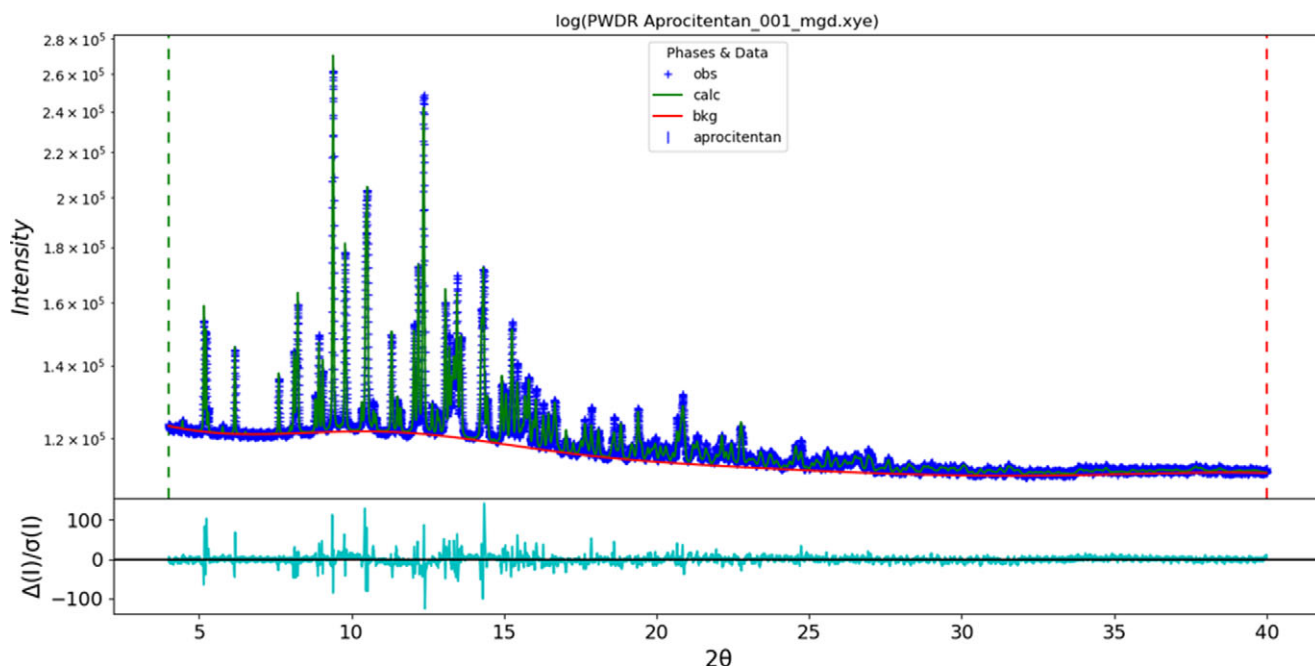


Figure 2. The Rietveld plot for aprocitentan Form A. The blue crosses represent the observed data points, and the green line is the calculated pattern. The cyan curve is the normalized error plot, and the red line is the background curve. The vertical scale is the logarithm of the counts.

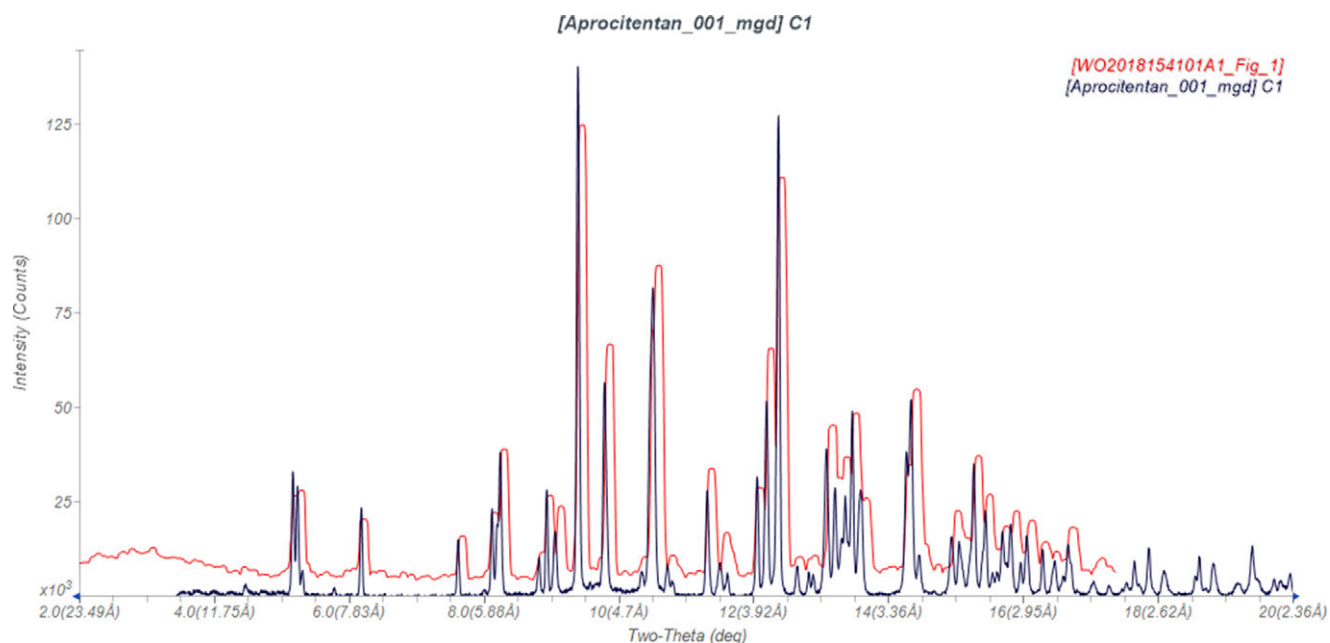


Figure 3. Comparison of the synchrotron pattern from this study of aprocitentan Form A (black) to that reported by Bolli et al. (2018) (red). The literature pattern (measured using Cu K α radiation) was digitized using UN-SCAN-IT (Silk Scientific, 2013) and converted to the synchrotron wavelength of 0.819826 (2) Å using JADE Pro (MDI, 2024). Image generated using JADE Pro (MDI, 2024).

(2018) (Figure 3) well enough to conclude that they represent the same material and, thus, that our sample is Form A.

The root-mean-square difference of the non-H atoms in the Rietveld-refined and VASP-optimized structures, calculated using the Mercury CSD-Materials/Search/Crystal Packing Similarity tool, is 0.334 Å (Figure 4). The root-mean-square Cartesian displacement of the non-H atoms in the

Rietveld-refined and VASP-optimized structures of the molecule, calculated using the Mercury Calculate/Molecule Overlay tool, is 0.297 Å (Figure 5). The agreements are at the upper end of the normal range for correct structures (van de Streek and Neumann, 2014). The largest difference is 0.823 Å at N11. Excluding this atom, the rms difference is 0.251 Å, and the main difference is in the orientation of the

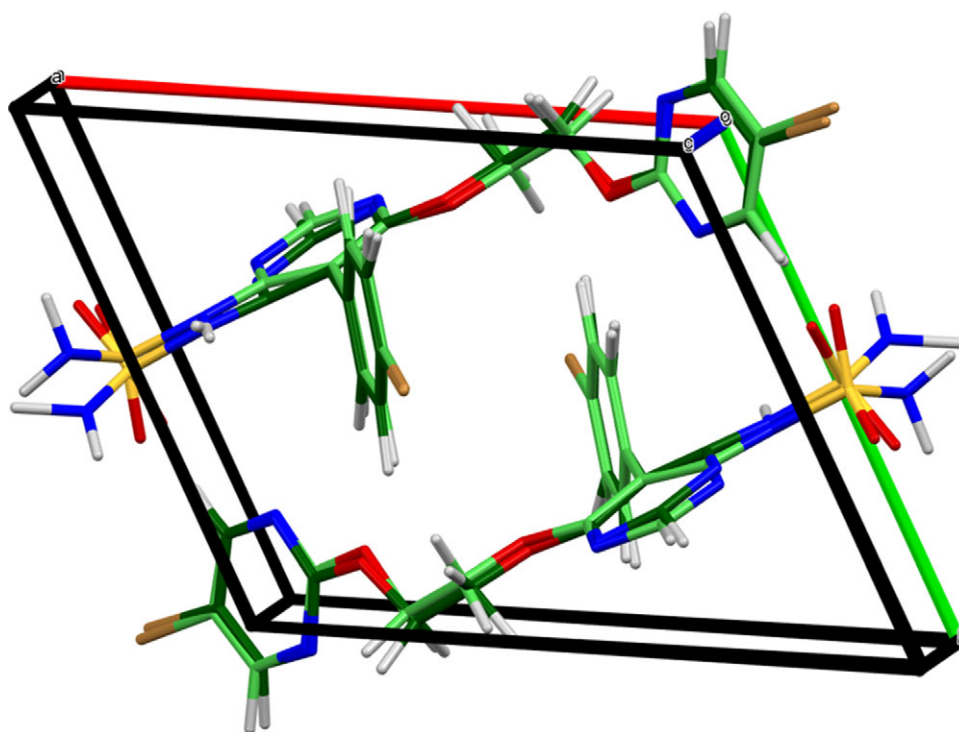


Figure 4. Comparison of the Rietveld-refined (colored by atom type) and VASP-optimized (light green) structures of aprocitentan Form A using the Mercury CSD-Materials/Search/Crystal Packing Similarity tool. The root-mean-square Cartesian displacement is 0.334 Å. Image generated using Mercury (Macrae et al., 2020).

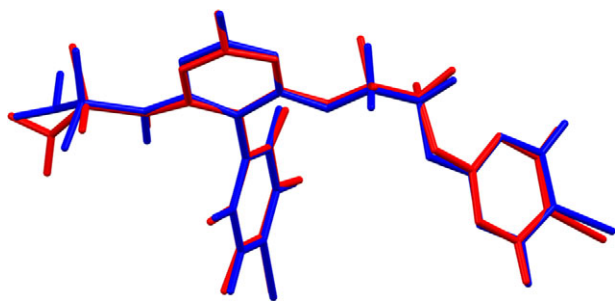


Figure 5. Comparison of the Rietveld-refined (red) and VASP-optimized (blue) structures of aprocitentan Form A using the Mercury Calculate/Molecule Overlay tool. The root-mean-square Cartesian displacement is 0.297 Å. Image generated using Mercury (Macrae et al., 2020).

SO₂ group; the agreement of the rest of the molecule is much better. The position and orientation of the sulfonamide group differ significantly between the refined and optimized structures. The asymmetric unit is illustrated in Figure 6. We will discuss both structures below.

All of the bond distances, bond angles, and most of the torsion angles in the refined structure fall within the normal ranges indicated by a Mercury Mogul Geometry check (Macrae et al., 2020). The torsion angles involving rotation about the S3–N8 bond lie slightly outside the *gauche/trans* distributions of a few similar torsion angles. In the VASP-optimized structure, the S3–N8 bond distance of 1.691 Å (average = 1.628(17) Å; Z-score = 3.7) and the N11–S3–N8 angle of 96.0° (average = 108.9(22)°; Z-score = 5.8) are flagged as unusual. The torsion angles involving rotation about the S3–N8 bond are likewise flagged as unusual. Too-long S–N bonds in the density functional theory (DFT) optimization of sulfonamides have been observed by others (Vibha et al., 2023). Even a more sophisticated VASP calculation (0.25 Å^{−1} *k*-point spacing, resulting in a 3 × 3 × 3 mesh, and including a DFT + D3 dispersion model) yielded the same geometry. One of us (J.A.K.) has previously encountered molecules for which the DFT-optimized geometry of a sulfonamide group was suspect. With the information currently

available to use, we do not know which (if either) of the two structures is correct. Since the purpose of this study is to generate a pattern for PDF[®], we report both structures and will let the reader decide which is appropriate.

Quantum chemical geometry optimizations of isolated aprocitentan molecule (DFT/B3LYP/6-31G*/water) using Spartan '24 (Wavefunction, Inc., 2023) indicated that the VASP-optimized molecule is lower in energy, but that both converge to a similar local minimum, which is more similar to the refined structure. The global minimum-energy conformation is much more compact (folded on itself), showing that intermolecular interactions are important to determining the solid-state conformation. The refined structure is more chemically reasonable.

The crystal structure (Figure 7) consists of layers of aprocitentan molecules, approximately along the 1,−7,7 plane. Hydrogen bonds (discussed below) link the molecules within these layers. The mean plane of the bromophenyl ring is approximately 5,−1,1, the mean plane of the bromopyrimidine ring is approximately 2,−1,1, and the mean plane of the pyrimidine ring is approximately −3,5,−1. The Mercury Aromatics Analyser indicates only weak interactions between the bromophenyl rings.

Analysis of the contributions to the total crystal energy of the structure using the Forcite module of Materials Studio (Dassault Systèmes, 2023) indicates that the intramolecular energy is dominated by angle distortion terms. The intermolecular energy is dominated by electrostatic attractions, which, in this force field-based analysis, also include hydrogen bonds.

A geometrical analysis of the refined structure indicates only one hydrogen bond (Table I). This N–H⋯N hydrogen bond links two molecules into a dimer, with a graph set (Etter, 1990; Bernstein et al., 1995; Motherwell et al., 2000) R2,2(8). The DFT-optimized structure contains two N–H⋯N hydrogen bonds (Table II), as well as a small number of non-classical hydrogen bonds.

The volume enclosed by the Hirshfeld surface of aprocitentan (Figure 8; Hirshfeld, 1977; Spackman et al., 2021) is

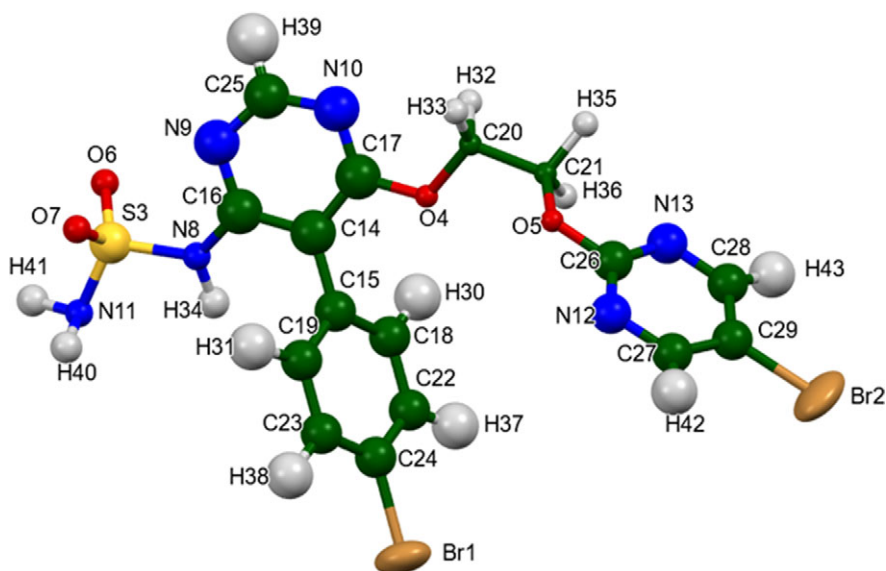


Figure 6. The asymmetric unit of aprocitentan Form A, with the atom numbering. The atoms are represented by 50% probability spheroids/ellipsoids. Image generated using Mercury (Macrae et al., 2020).

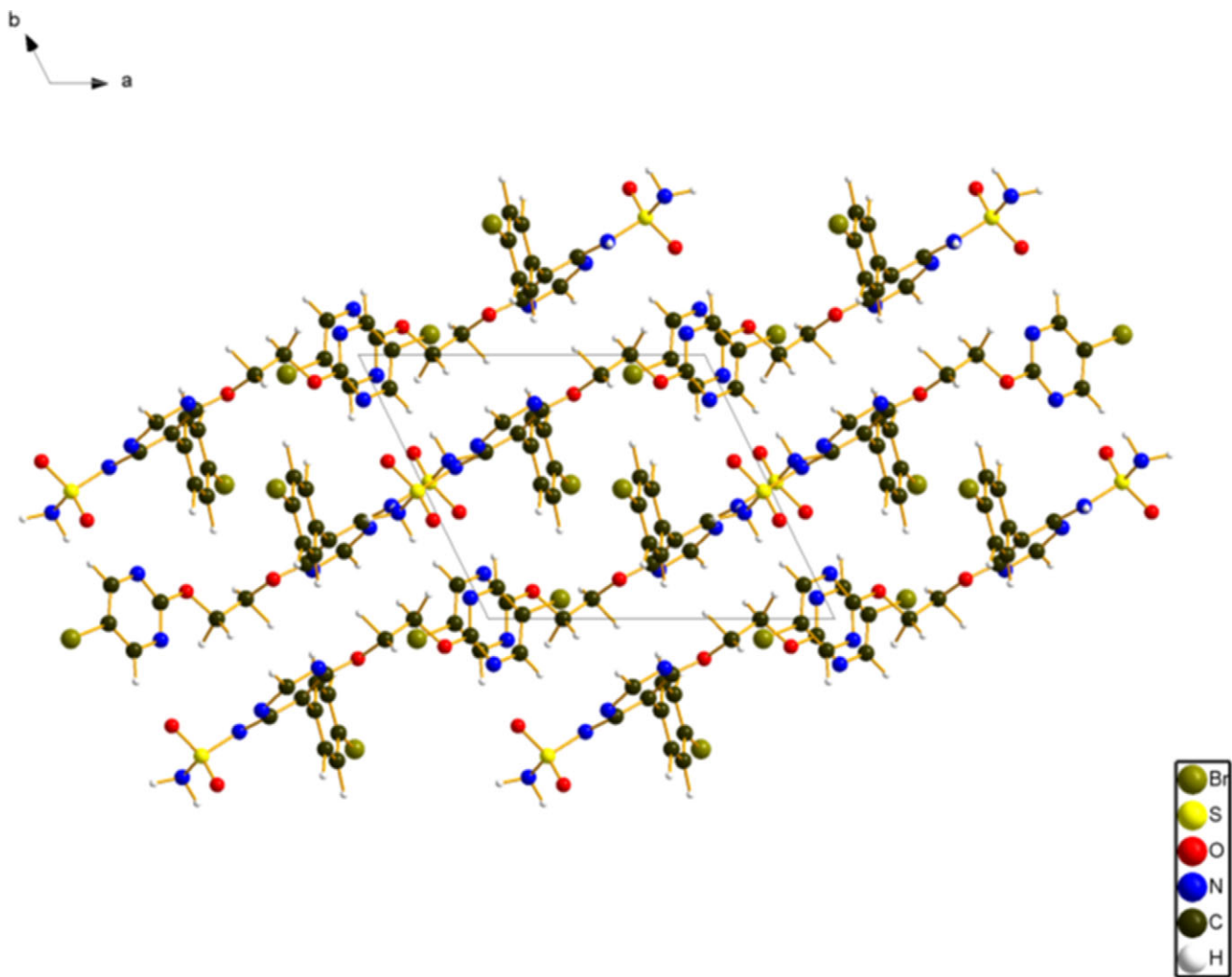


Figure 7. The crystal structure of aprocitentan Form A, viewed down the *c*-axis. Image generated using Diamond (Crystal Impact, 2023).

TABLE I. Hydrogen bond in the Rietveld-refined structure of aprocitentan

H bond	D–H, Å	H···A, Å	D···A, Å	D–H···A, °
N8–H34···N11	1.026	2.012	3.044	179.6

498.90 Å³, which is 98.06% of half the unit cell volume. The packing density is thus typical. The only significant close contacts (red in Figure 8) involve the hydrogen bonds. The volume/non-hydrogen atom is typical at 17.5 Å³.

The Bravais–Friedel–Donnay–Harker (Bravais, 1866; Friedel, 1907; Donnay and Harker, 1937) algorithm suggests that we might expect isotropic morphology for aprocitentan.

A second-order spherical harmonic model was included in the refinement. The texture index was 1.010(0), indicating that the preferred orientation was insignificant in this rotated capillary specimen.

ACKNOWLEDGEMENTS

We thank Adam Leontowich for his assistance in the data collection. We also thank the ICDD team – Megan Rost, Steve Trimble, and Dave Bohnenberger – for their contribution to research, sample preparation, and in-house XRD data collection and verification.

TABLE II. Hydrogen bonds (VASP/CRYSTAL23) in the optimized structure of aprocitentan. * = intramolecular

H bond	D–H, Å	H···A, Å	D···A, Å	D–H···A, °	Mulliken overlap, <i>e</i>
N11–H41···N12	1.047	1.944	2.964	163.9	0.059
N11–H41···S3	1.047	2.247*	1.660	43.9	0.016
N8–H34···N11	1.030	2.179	3.196	169.3	0.041
N11–H40···C22	1.028	2.553	3.567	168.9	0.012
C27–H42···O7	1.094	2.325	3.321	150.5	0.022
C23–H38···O5	1.089	2.457	3.357	139.2	0.014

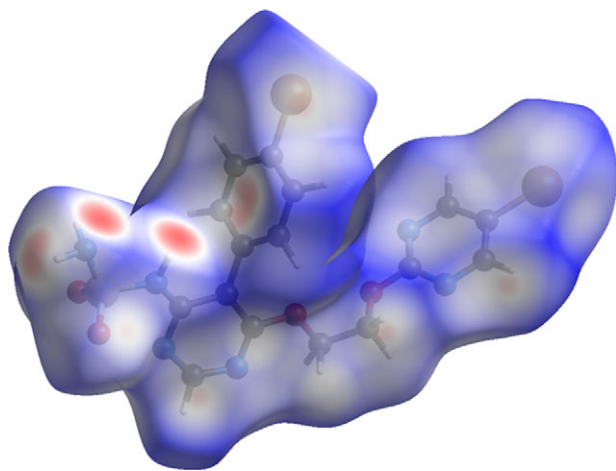


Figure 8. The Hirshfeld surface of aprocitentan Form A. Intermolecular contacts longer than the sums of the van der Waals radii are colored blue, and contacts shorter than the sums of the radii are colored red. Contacts equal to the sums of radii are white. Image generated using CrystalExplorer (Spackman et al., 2021).

DATA AVAILABILITY STATEMENT

The powder pattern of aprocitentan from this synchrotron dataset has been submitted to the International Centre for Diffraction Data (ICDD) for inclusion in PDF[®]. The Crystallographic Information Framework (CIF) files containing the results of the Rietveld refinement (including the raw data) and the DFT geometry optimization were deposited with the ICDD. The data can be requested at pdj@icdd.com.

FUNDING STATEMENT

Part or all of the research described in this paper was performed at the Canadian Light Source, a national research facility of the University of Saskatchewan, which is supported by the Canada Foundation for Innovation (CFI), the Natural Sciences and Engineering Research Council (NSERC), the Canadian Institute of Health Research (CIHR), the Government of Saskatchewan, and the University of Saskatchewan. This work was partially supported by the International Centre for Diffraction Data.

CONFLICTS OF INTEREST

The authors have no conflicts of interests to declare.

REFERENCES

- Altomare, A., C. Cuocci, C. Giacovazzo, A. Moliterni, R. Rizzi, N. Corriero, and A. Falcicchio. 2013. "EXPO2013: A Kit of Tools for Phasing Crystal Structures from Powder Data." *Journal of Applied Crystallography* 46: 1231–5.
- Bernstein, J., R. E. Davis, L. Shimon, and N. L. Chang. 1995. "Patterns in Hydrogen Bonding: Functionality and Graph Set Analysis in Crystals." *Angewandte Chemie International Edition in English* 34: 1555–73.
- Bibulić, P. and M. Matečić. 2021. "Solid State Forms of Aprocitentan and Process for Preparation Thereof." International Patent Application WO 2021/237004 A1.
- Bolli, M., C. Boss, and A. Treiber. 2012. "4-Pyrimidinesulfamide Derivative." U.S. Patent US 8324232 B2.
- Bolli, M., P. Kohler, I. Schindelholz, and M. Von Raumer. 2018. "Crystalline Forms of the 4-Pyrimidinesulfamide Derivative Aprocitentan." International Patent Application WO 2018/154101 A1.
- Bolli, M., Kohler, P., I. Schindelholz, and M. Von Raumer. 2020. "Crystalline Forms of a 4-Pyrimidinesulfamide Derivative Aprocitentan." U.S. Patent Application US 2020/0002317 A1.
- Bravais, A. 1866. *Etudes Cristallographiques*. Paris: Gauthier Villars.
- Bruno, I. J., J. C. Cole, M. Kessler, J. Luo, W. D. S. Motherwell, L. H. Purkis, B. R. Smith, et al. 2004. "Retrieval of Crystallographically-Derived Molecular Geometry Information." *Journal of Chemical Information and Computer Sciences* 44: 2133–44.
- Chen, M., and H. Zhu. 2021. "Crystal Form of Aprocitentan, Preparation Method Therefor and Use Thereof." International Patent Application WO 2021/088645 A1.
- Crystal Impact. 2023. *Diamond V. 5.0.0*, edited by Dr. H. Putz & Dr. K. Brandenburg. Bonn: Crystal Impact.
- Dassault Systèmes. 2023. *BIOVIA Materials Studio 2024*. San Diego, CA: BIOVIA.
- Donnay, J. D. H., and D. Harker. 1937. "A New Law of Crystal Morphology Extending the Law of Bravais." *American Mineralogist* 22: 446–67.
- Erba, A., J. K. Desmarais, S. Casassa, B. Civalieri, L. Donà, I. J. Bush, B. Searle, et al. 2023. "CRYSTAL23: A Program for Computational Solid State Physics and Chemistry." *Journal of Chemical Theory and Computation* 19: 6891–932; <https://doi.org/10.1021/acs.jctc.2c00958>.
- Etter, M. C. 1990. "Encoding and Decoding Hydrogen-Bond Patterns of Organic Compounds." *Accounts of Chemical Research* 23: 120–6.
- Friedel, G. 1907. "Etudes sur la loi de Bravais." *Bulletin de la Société Française de Minéralogie* 30: 326–455.
- Gatti, C., V. R. Saunders, and C. Roetti. 1994. "Crystal-Field Effects on the Topological Properties of the Electron-Density in Molecular Crystals – the Case of Urea." *Journal of Chemical Physics* 101: 10686–96.
- Groom, C. R., I. J. Bruno, M. P. Lightfoot, and S. C. Ward. 2016. "The Cambridge Structural Database." *Acta Crystallographica Section B: Structural Science, Crystal Engineering and Materials* 72: 171–9.
- Hirshfeld, F. L. 1977. "Bonded-Atom Fragments for Describing Molecular Charge Densities." *Theoretica Chimica Acta* 44: 129–38.
- Kabekkodu, S., A. Dosen, and T. N. Blanton. 2024. "PDF-5+: A Comprehensive Powder Diffraction File™ for Materials Characterization." *Powder Diffraction* 39: 47–59.
- Kaduk, J. A., C. E. Crowder, K. Zhong, T. G. Fawcett, and M. R. Suchomel. 2014. "Crystal Structure of Atomoxetine Hydrochloride (Strattera), C₁₇H₂₂NOCl." *Powder Diffraction* 29: 269–73.
- Kim S., J. Chen, T. Cheng, A. Gindulyte, J. He, S. He, Q. Li, et al. 2023. "PubChem 2023 Update." *Nucleic Acids Research* 51 (D1): D1373–D1380. <https://doi.org/10.1093/nar/gkac956>.
- Kresse, G., and J. Furthmüller. 1996. "Efficiency of Ab-Initio Total Energy Calculations for Metals and Semiconductors Using a Plane-Wave Basis Set." *Computational Materials Science* 6: 15–50.
- Leontowich, A. F. G., A. Gomez, B. Diaz Moreno, D. Muir, D. Spasyuk, G. King, J. W. Reid, C.-Y. Kim, and S. Kycia. 2021. "The Lower Energy Diffraction and Scattering Side-Bounce Beamline for Materials Science at the Canadian Light Source." *Journal of Synchrotron Radiation* 28: 1–9. <https://doi.org/10.1107/S1600577521002496>.
- Macrae, C. F., I. Sovago, S. J. Cottrell, P. T. A. Galek, P. McCabe, E. Pidcock, M. Platings, et al. 2020. "Mercury 4.0: From Visualization to Design and Prediction." *Journal of Applied Crystallography* 53: 226–35.
- Materials Design. 2024. *Medea 3.7.2*. San Diego, CA: Materials Design Inc.
- MDI. 2024. *JADE Pro Version 9.0*. Livermore, CA: Materials Data.
- Motherwell, W. D. S., G. P. Shields, and F. H. Allen. 2000. "Graph-Set and Packing Analysis of Hydrogen-Bonded Networks in Polyamide Structures in the Cambridge Structural Database." *Acta Crystallographica B* 56: 857–71.
- Peintinger, M. F., D. Vilela Oliveira, and T. Bredow. 2013. "Consistent Gaussian Basis Sets of Triple-Zeta Valence with Polarization Quality for Solid-State Calculations." *Journal of Computational Chemistry* 34: 451–9.
- Silk Scientific. 2013. *UN-SCAN-IT 7.0*. Orem, UT: Silk Scientific Corporation.
- Spackman, P. R., M. J. Turner, J. J. McKinnon, S. K. Wolff, D. J. Grimwood, D. Jayatilaka, and M. A. Spackman. 2021. "CrystalExplorer: A Program for Hirshfeld Surface Analysis, Visualization and Quantitative Analysis of Molecular Crystals." *Journal of Applied Crystallography* 54: 1006–11. <https://doi.org/10.1107/S1600576721002910>; <https://crystalexplor.net>.

- Sykes, R. A., P. McCabe, F. H. Allen, G. M. Battle, I. J. Bruno, and P. A. Wood. 2011. "New Software for Statistical Analysis of Cambridge Structural Database Data." *Journal of Applied Crystallography* 44: 882–6.
- Toby, B. H., and R. B. Von Dreele. 2013. "GSAS II: The Genesis of a Modern Open-Source All Purpose Crystallography Software Package." *Journal of Applied Crystallography* 46: 544–9.
- van de Streek, J., and M. A. Neumann. 2014. "Validation of Molecular Crystal Structures from Powder Diffraction Data with Dispersion-Corrected Density Functional Theory (DFT-D)." *Acta Crystallographica Section B: Structural Science, Crystal Engineering and Materials* 70: 1020–32.
- Vibha, K., N. C. Prachality, R. A. Reddy, M. N. Ravikantha, and J. Thippurudrappa. 2023. "Computational Studies on Sulfonamide Drug Molecules by Density Functional Theory." *Chemical Physics Impact* 6: 100147. <https://doi.org/10.1016/j.chphi.2022.100147>.
- Wavefunction, Inc. 2023. *Spartan '24. V. 1.0.0*. Irvine, CA: Wavefunction, Inc.